Shocks near Jamming

Gómez, L.R.; Turner, A.M.; van Hecke, M.; Vitelli, V.

DOI
10.1103/PhysRevLett.108.058001
Publication date
2012
Document Version
Final published version
Published in
Physical Review Letters

Shocks near Jamming

Leopoldo R. Gómez,[1,*] Ari M. Turner,[2] Martin van Hecke,[3] and Vincenzo Vitelli[1,†]

[1]*Instituut-Lorentz, Universiteit Leiden, P.O. Box 9056, 2300 RA Leiden, The Netherlands*

[2]*Department of Physics, University of California, Berkeley, California 94720, USA*

[3]*Kamerlingh Onnes Lab, Universiteit Leiden, Postbus 9504, 2300 RA Leiden, The Netherlands*

(Received 19 September 2011; revised manuscript received 17 November 2011; published 31 January 2012)

Nonlinear sound is an extreme phenomenon typically observed in solids after violent explosions. But granular media are different. Right when they jam, these fragile and disordered solids exhibit a vanishing rigidity and sound speed, so that even tiny mechanical perturbations form supersonic shocks. Here, we perform simulations in which two-dimensional jammed granular packings are dynamically compressed and demonstrate that the elementary excitations are strongly nonlinear shocks, rather than ordinary phonons. We capture the full dependence of the shock speed on pressure and impact intensity by a surprisingly simple analytical model.

DOI: 10.1103/PhysRevLett.108.058001 PACS numbers: 81.05.Rm, 43.25.+y, 46.40.Cd

Granular materials exhibit a wide range of complex collective behaviors, making them an important testing ground for the physics of amorphous materials [1–16]. The confining pressure P is perhaps the most important parameter controlling their properties. Strongly compressed granular media are, in many aspects, simple solids in which perturbations travel as ordinary phonons. However, when the confining pressure is lowered to zero or the amplitude of the disturbance is much higher than the initial compression, the mechanical response of granular media becomes increasingly anomalous.

Several insights have been obtained by studying a simple model of granular media comprised of soft frictionless spheres just above the jamming point [1–16]. The jamming point corresponds to the critical density at which the grains barely touch and P vanishes [1]. The first insight is that the vibrational modes of jammed packings resemble ordinary phonons only below a characteristic frequency scale ω^* that vanishes as P goes to zero [3–5]. Above ω^*, the modes are extended but strongly scattered by disorder [13–15]. Second, as a direct consequence of the nonlinear dependence of the local contact force on the grain deformations, the sound speed vanishes as P goes to zero [7–15]: linear sound cannot propagate when the particles barely touch. Third, the range of validity of linear response vanishes when P goes to zero. This is intuitive since the material is about to fall apart when the pressure vanishes [16].

As the pressure (or density) is lowered towards the jamming point, there are thus three anomalies that forbid the propagation of ordinary phonons: disorder disrupts phononic transport for all frequency scales, the sound speed vanishes, and linear response is no longer valid. The vanishing of the sound speed and absence of a linear range clearly suggest that the excitations near jamming will be strongly nonlinear. Nevertheless, most numerical and analytical studies of energy transport have been carried out in solids just above the jamming point, within a vanishingly small window of linear response. By explicit design, these studies cannot probe nonlinear energy transport because the dynamics of the system is solved through a normal mode expansion [12–15]. Therefore, with the exception of theoretical and experimental studies on solitons in one-dimensional granular chains, started with the seminal work of Nesterenko [17–21], nonlinear energy transport in granular packings remains largely unexplored.

Numerical model.—To probe how elastic energy is transported close to the jamming point, we performed molecular dynamics simulations of a piston-compression experiment carried out in two-dimensional polydisperse amorphous packings of soft frictionless spheres, whose radii, R_i, are uniformly distributed between 0.8 and 1.2 times their average R. Particles i and j at positions $\vec{x}_i$ and $\vec{x}_j$ interact via a nonlinear repulsive contact potential [12]

$$V_{ij} = \frac{\varepsilon_{ij}}{\alpha}\delta_{ij}{}^{\alpha} \tag{1}$$

only for positive overlap $\delta_{ij} \equiv R_i + R_j - |\vec{x}_i - \vec{x}_j| > 0$; otherwise, $V_{ij} = 0$ when $\delta_{ij} \leq 0$. Here, the interaction parameter $\varepsilon_{ij} = \frac{4}{3}\frac{R_i R_j}{R_i + R_j} E^*_{ij}$ is expressed in terms of the effective Young's modulus of the two particles, E^*_{ij}; see Ref. [12] for more details. The case $\alpha = 5/2$ corresponds to Hertz's law. Lengths are measured in units of average particle diameter. The unit of mass is set by fixing the grain density to unity. The effective particle Young modulus E^* is set to one, which becomes the pressure unit. These choices ensure that the speed of sound *inside* the grain, v_g, is one [12].

We prepare Hertzian packings at a fixed pressure P, or equivalently, an average particle overlap $\delta_0 \sim P^{2/3}$. They are then continuously compressed by a piston which moves with a constant velocity u_P in the x direction throughout the simulation; see Fig. 1. The subsequent motion of the particles is obtained by numerical integration of Newton's

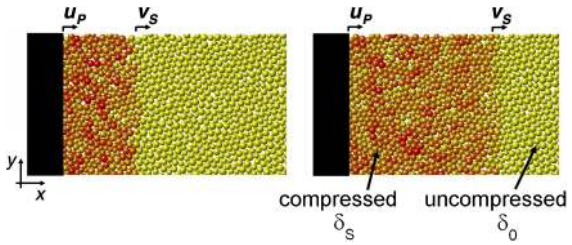

FIG. 1 (color online). Snapshots of the piston-compression simulation. A massive piston moves to the right at a constant velocity u_P, resulting in the formation of a compression front traveling at a speed v_S. Color indicates the local pressure at each grain. The average particle overlap is δ_0 to the right of the front and $\delta_S > \delta_0$ to the left.

equations of motion subject to periodic boundary conditions in the y direction and a fixed boundary on the right edge of the system. We use two-dimensional packings in the range of 10^3 to 10^4 particles with various width-to-length ratios.

Phenomenology.—The piston compression leads to the formation of a front that separates two states. Ahead of the front, we find a region where the particles are at rest having the initial overlap δ_0, whereas behind it there is a compressed region with particles moving on average with the piston speed u_P and an overlap $\delta_S > \delta_0$. Figure 2(a) shows typical profiles for the *longitudinal* particle velocity u (in the $\hat{x}$ direction) as a function of x, obtained upon averaging velocity fluctuations in the $\hat{y}$ direction.

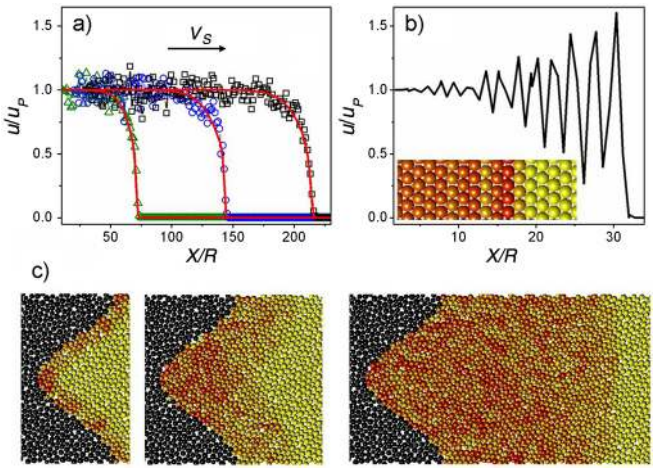

FIG. 2 (color online). (a) Profiles of a shock wave at different times obtained by averaging the particle velocity in the $\hat{y}$ direction (symbols). The lines shows the fits of the fronts to an empirical fit formula. (b) Oscillatory velocity profile of a shock-like wave propagating through a hexagonal array. The inset shows the in-phase motion of the crystalline planes that gives rise to the pressure oscillations. (c) Representative snapshots of the focusing and flattening of an initially curved front generated by a sinusoidal piston (time progresses from left to right).

Two qualitative features of the shocks stand out for all the amorphous packings probed in this study: the fronts are smooth and stable. The smoothness can be contrasted with the typical shock profile that arises in ordered lattices of grains. Figure 2(b), obtained for a triangular lattice of grains with zero initial overlap, shows large coherent pressure oscillations caused by the in-phase motion of the crystalline planes. These peaks are washed out by disorder in the amorphous packings.

Second, we have systematically tested the stability of the front against sinusoidal perturbations (in the y direction) of varying amplitudes and wavelengths in disordered packings under various pressures. This was done through directs simulations [22], as well as by performing a Dyakov's stability analysis [22–24]. A typical result from our simulations, illustrated in Fig. 2(c), shows how the front remains stable due to a classic stress focusing process, where particles "left behind" experience a large compression, pushing them to catch up with the rest of the front. In light of these observations, the shocks can be treated as one-dimensional front propagation phenomena.

Front speed.—Once transients have died out, the front propagates with constant speed v_S in the amorphous packings. Upon using conservation of mass across the shock front, we derive a one-dimensional relation between the characteristic velocities u_P and v_S, through the average radius of the particles, R, and the average compression in the shock, δ_S, and ahead of it, δ_0:

$$v_S = u_P \frac{2R - \delta_0}{\delta_S - \delta_0}. \tag{2}$$

Since the particle compression δ_S is typically much less than its diameter $2R$, Eq. (2) implies that $v_S \gg u_P$. This is consistent with our numerical findings, summarized in Fig. 3(a), where the dependence of v_S on u_P is explored systematically for different compressions.

Inspection of Fig. 3(a) reveals two distinct regimes. For low u_P, the front speed v_S is nearly independent of u_P—in this (quasi)linear regime, v_S is simply controlled by the initial pressure P. The strongly nonlinear shock wave regime is reached for the high compression speed u_P, where v_S depends on u_P but not on P.

The data for v_S can be collapsed onto a single master curve, as shown in Fig. 3(b). We achieve this upon rescaling the v_S axis by $v_S(0)$, the numerically determined value that the front speed attains in the limit of vanishing u_P [see Fig. 3(a)]. The u_P axis is rescaled by a pressure-dependent velocity scale u_P^*, obtained by matching the low and high u_P asymptotes in Fig. 3(a) (see arrow): u_P^* marks the crossover between linear acoustic waves and shocks.

Scaling analysis.—The pressure dependence of $v_S(0)$ can be rationalized using scaling arguments. We expect that $v_S(0)$ reduces to c, the speed of linear longitudinal sound waves. To determine the scaling of c with pressure, note that $c \sim \sqrt{B}$, where the bulk modulus $B = \frac{\partial P}{\partial V}$ and

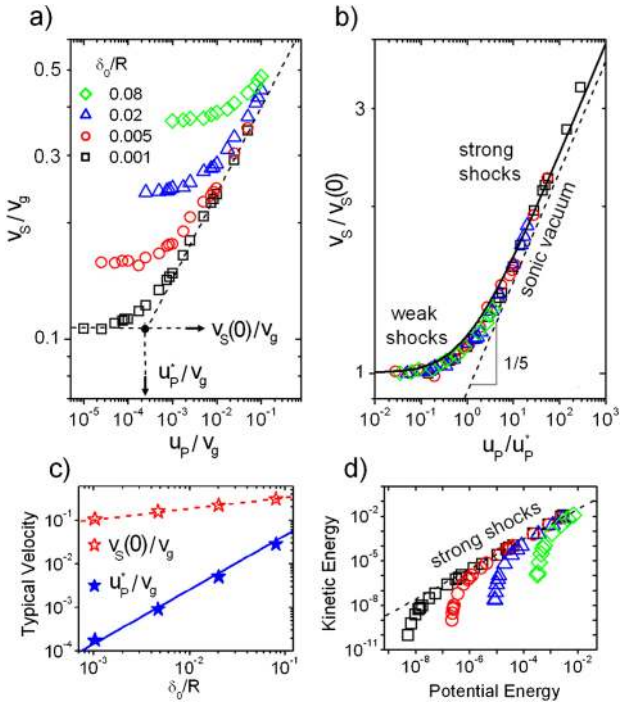

FIG. 3 (color online). (a) Speed of the front v_S versus particle velocity u_P measured in units of v_g, the sound speed within the grain, for decreasing particle overlap δ_0. (b) Same plot as in (a) but with v_S normalized by $v_S(0)$ and u_P normalized by the crossover particle speed u_P^*: $v_S(0)$ and u_P^* are indicated in (a). The dashed line indicates the power law $v_S \sim u_P^{1/5}$ characteristic of a sonic vacuum. The solid line indicates the theory developed here to describe the universal transition from weakly to strongly nonlinear waves in systems close to jamming. (c) Variation of $v_S(0)$ and u_P^* with distance to the jamming transition parametrized by the initial average overlap δ_0. The dashed line indicates the power law $v_S(0) \sim \delta_0^{1/4}$ and the continuous line the power law $u_P^* \sim \delta_0^{5/4}$. (d) Variation of the kinetic energy with potential energy in dimensionless units—same color code as in (a),(b). The dashed line indicates the linear relationship observed for strong shocks.

$P = \frac{\partial E}{\partial V}$. The change in volume dV scales linearly with δ_0, the average overlap between particles, while the energy scales as $E \sim \delta_0^\alpha$; see Eq. (1). Upon setting $\alpha = 5/2$, we obtain the pressure dependence of the longitudinal speed of sound $c \sim \delta_0^{1/4} \sim P^{1/6}$ valid for Hertzian interactions [12]. Figure 3(c) shows that the numerical data for $v_S(0)$, represented by open symbols, are consistent with the $\delta_0^{1/4}$ scaling, which is shown as a dashed line.

We now turn to the regime of high piston speeds, $u_P \gg u_P^*$, when the front speed v_S becomes nearly independent of P. Since u_P, R, and δ_0 are all known, we need one additional relation which, combined with Eq. (2), will make a definite prediction for the shock speed. We note that, for strong shocks, the propagating front generates a characteristic compression $\delta \gg \delta_0$ and a corresponding increase in the kinetic energy. By assuming that the kinetic and potential energies are of the same order, we obtain $u_P^2 \sim \delta^{5/2}$. We have tested numerically that this nontrivial proportionality relation exists for strong deformations; see Fig. 3(d). Upon combining the balance between kinetic and potential energy with Eq. (2), one readily obtains the power law $v_S \sim u_P^{1/5}$, plotted as a dashed line in Fig. 3(b). This scaling relation is clearly consistent with our numerical data for the speed of strongly nonlinear shock waves.

We deduce the dependence on compression of the crossover speed u_P^* by smoothly matching the two asymptotic relations for the front speed $v_S \sim u_P^{1/5}$ and $v_S(0) \sim \delta_0^{1/4}$. This leads to the power law relation $u_P^* \sim \delta_0^{5/4}$ [continuous line in Fig. 3(c)] that is consistent with our numerical values (filled symbols). Note that the data collapse in Fig. 3(b) depends only on the scaling $u_P^* \sim \delta_0^{5/4}$ and is not sensitive on the precise definition of the crossover speed. Upon using the conversion relation $u_P \sim \delta^{5/4}$, the intuitive expectation that the crossover takes place when $\delta \approx \delta_0$ is confirmed.

We conclude that, by controlling δ_0 or P, which parametrize the distance to the jamming point (at $P = 0$ and $\delta_0 = 0$), we can tune u_P^* and the onset of the strongly nonlinear response of the packings. Our key numerical findings on the shock velocity, summarized in Fig. 3, can be grasped from scaling near the jamming point.

Analytical model.—In order to account for the dependence of v_S on u_P and the smoothness of the shock profiles, we construct the simplest possible one-dimensional model that quantitatively accounts for the trends observed in Fig. 3 and sheds light on the role of disorder.

In the continuum limit, we obtain the following equation governing the dynamics of the system in terms of the strain field $\delta(x, t)$ [25]:

$$\frac{R^2}{3}\delta_{ttxx} - \delta_{tt} + \frac{4R^2\varepsilon}{m}[\delta^{\alpha-1}]_{xx} = 0. \tag{3}$$

To gain some intuition for the physics behind Eq. (3), note that, by setting $\alpha = 2$, one recovers a linear dispersive wave equation, with speed proportional to $\sqrt{\varepsilon/m}$ in the long wavelength limit. By contrast, when $\alpha > 2$, a nonlinear wave equation is obtained. Nonlinearities and dispersive effects gives rise to finite amplitude waves: either solitary waves or shocks are possible depending on the drive [18].

Shock propagation is modeled by the combined strain $\delta(x, t) = \delta_0 + g(\tilde{x})$, where $g(\tilde{x})$ gives the shape of the shock and $\tilde{x} \equiv x - v_S t$. Upon inserting this ansatz into Eq. (3), we obtain the conservation law $\frac{1}{2}\delta_{\tilde{x}}^2 + W(\delta) = 0$, where $W(\delta)$ is given by

$$W(\delta) = \frac{24\varepsilon}{m\alpha v_S^2}(\delta^\alpha - \delta_0^\alpha) - \frac{3}{R^2}(\delta^2 - \delta_0^2) - 24\delta_0\left(\frac{\varepsilon}{mv_S^2}\delta_0^{\alpha-2} - \frac{1}{4R^2}\right)(\delta - \delta_0). \tag{4}$$

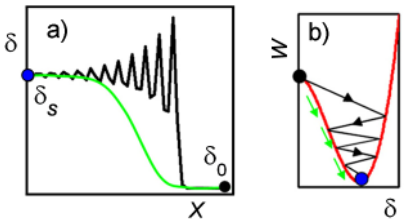

FIG. 4 (color online). (a) Simulations of an ordered chain with small viscosity display large coherent oscillations in the front profile (black line) [26]. If the viscosity is large enough, one obtains a homogeneous shock profile, shown as a light gray (green) line, similar to the profile in Fig. 2(a). (b) The presence of an *effective* viscosity will induce the oscillation of the particle (represented by thin black lines) towards the bottom of the potential $W(\delta)$. If the viscosity is large enough, the particle can move directly to the minimum without performing any oscillations; see the light gray (green) trajectory corresponding to the homogeneous shock profile of (a).

This conservation law can be interpreted as describing the total energy of an effective particle at position δ rolling down a potential well $W(\delta)$, shown in Fig. 4(b) (here $\tilde{x}$ maps to time so that $\frac{1}{2}\dot{\delta}_{\tilde{x}}^2$ is the kinetic term of the particle) [26].

One of the key ideas of our Letter is that disorder can act as an effective viscosity for the shock: the energy imparted unidirectionally by the piston is redistributed among other degrees of freedom, reducing the energy propagating with the shock front. In our mapping, this implies that the effective particle, initially located at the maximum of the potential $W = 0$, moves to the minimum of the potential well [see Fig. 4(a)]. Thus, upon setting $\partial_\delta W(\delta) = 0$, we can obtain a relation between propagation velocity and induced compression in the front

$$\frac{v_S}{c} = \sqrt{\frac{1}{\alpha - 1}\frac{(\delta_S/\delta_0)^{\alpha-1} - 1}{(\delta_S/\delta_0) - 1}} \tag{5}$$

that is independent of viscosity, even if an infinitesimal amount of dissipation is necessary to obtain a steady state solution of Eq. (3).

Together, Eqs. (2) and (5) can be seen as a parametric relation between front and particle velocities, where the overlap δ_S produced by the passage of the front is the parameter. Such a parametric plot of v_S versus u_P is drawn as a continuous curve on the numerical data in Fig. 3(b). This comparison shows that Eqs. (2) and (5) are in excellent agreement (without any fitting parameter) with the results of our numerical experiments on shock propagation.

Discussion.—The shock formation explored in the present study is a generic phenomenon independent of the dimensionality of the sample that relies purely on the presence of a nonlinear law between grains (for any $\alpha > 2$) and not on the presence of friction. Experimentally, this can be tested by impacting a box of (frictional) glass beads with a heavy mass, for a range of impact speeds and pressures—preliminary experimental results for the front speed compare favorably to our theoretical predictions in Fig. 3 [27].

We note, however, that, in frictional granular media, a second type of densification front can be observed, which is often referred to as plowing [9,10]. Whereas our shock waves always propagate with speeds above the linear sound speed and continue to propagate even after the driving stops, plowing fronts are generally much slower (in [9], of the order of 1 m/s) and stop almost immediately when the driving stops. We believe that the underlying difference is that our shocks are dynamical phenomena, set by a balance of potential and kinetic energies, whereas plowing is in essence a quasistatic phenomenon, dominated by dissipation. In the dynamic case, the change in packing fraction induced by the shock is associated with grain deformations, whereas, in the quasistatic case, densification is dominated by grain rearrangements and compaction.

Outlook.—The shocks that arise in grains near jamming are just one representative of a broader class of strongly nonlinear excitations that emerge near the marginal state of suspensions, emulsions, wet foams, and weakly connected fiber networks [6,28,29]. Close to losing their rigidity, all these materials exhibit a vanishing range of linear response, so that almost any amount of finite driving will elicit an extreme mechanical response in the form of rearrangements, yielding, and flow [16,30–32]. It remains an open question whether all these phenomena can be successfully described in terms of simple scaling near jamming.

We acknowledge inspiring discussions with X. Campman, V. Nesterenko, W. van Saarloos, A. Tichler, and N. Upadhyaya. L. R. G. and A. M. T. acknowledge financial support from FOM and Shell.

*gomez@lorentz.leidenuniv.nl
†vitelli@lorentz.leidenuniv.nl

[1] C. S. O'Hern, L. E. Silbert, A. J. Liu, and S. R. Nagel, Phys. Rev. E **68**, 011306 (2003).
[2] L. E. Silbert, A. J. Liu, and S. R. Nagel, Phys. Rev. Lett. **95**, 098301 (2005).
[3] M. Wyart, S. R. Nagel, and T. A. Witten, Europhys. Lett. **72**, 486 (2005).
[4] W. G. Ellenbroek, E. Somfai, M. van Hecke, and W. van Saarloos, Phys. Rev. Lett. **97**, 258001 (2006).
[5] A. Souslov, A. J. Liu, and T. C. Lubensky, Phys. Rev. Lett. **103**, 205503 (2009).
[6] M. van Hecke, J. Phys. Condens. Matter **22**, 033101 (2010).
[7] C. H. Liu and S. R. Nagel, Phys. Rev. Lett. **68**, 2301 (1992).
[8] X. Jia, C. Caroli, and B. Velicky, Phys. Rev. Lett. **82**, 1863 (1999).

[9] J. R. Royer, B. Conyers, E. I. Corwin, P. J. Eng, and H. M. Jaeger, Europhys. Lett. **93**, 28 008 (2011).
[10] M. M. Bandi, T. Tallinen, and L. Mahadevan, Europhys. Lett. **96**, 36 008 (2011).
[11] H. A. Makse, N. Gland, D. L. Johnson, and L. Schwartz, Phys. Rev. E **70**, 061302 (2004).
[12] E. Somfai, J. N. Roux, J. H. Snoeijer, M. van Hecke, and W. van Saarloos, Phys. Rev. E **72**, 021301 (2005).
[13] N. Xu, V. Vitelli, M. Wyart, A. J. Liu, and S. R. Nagel, Phys. Rev. Lett. **102**, 038001 (2009).
[14] V. Vitelli, N. Xu, M. Wyart, A. J. Liu, and S. R. Nagel, Phys. Rev. E **81**, 021301 (2010).
[15] M. Wyart, Europhys. Lett. **89**, 64 001 (2010).
[16] N. Xu, V. Vitelli, A. J. Liu, and S. R. Nagel, Europhys. Lett. **90**, 56 001 (2010).
[17] V. F. Nesterenko, J. Appl. Mech. Tech. Phys. **24**, 733 (1984).
[18] V. F. Nesterenko, *Dynamics of Heterogeneous Materials* (Springer-Verlag, New York, 2001).
[19] S. Sen, J. Hong, J. Bang, E. Avalos, and R. Doney, Phys. Rep. **462**, 21 (2008).
[20] A. Spadoni and C. Daraio, Proc. Natl. Acad. Sci. U.S.A. **107**, 7230 (2010).
[21] N. Boechler, G. Theocharis, and C. Daraio, Nature Mater. **10**, 665 (2011).
[22] L. Gomez *et al.* (to be published).
[23] S. P. Dyakov, Zh. Eksp. Teor. Fiz. **27**, 288 (1954).
[24] G. H. Swan and G. R. Fowles, Phys. Fluids **18**, 28 (1975).
[25] Equation (3) is simpler than the one originally introduced by Nesterenko [18].
[26] E. B. Herbold and V. F. Nesterenko, Phys. Rev. E **75**, 021304 (2007).
[27] S. van den Wildenberg, R. van Loo, and M. van Hecke (to be published).
[28] M. Wyart, H. Liang, A. Kabla, and L. Mahadevan, Phys. Rev. Lett. **101**, 215501 (2008).
[29] C. P. Broedersz, X. Mao, T. C. Lubensky, and F. C. MacKintosh, Nature Phys. **7**, 983 (2011).
[30] B. P. Tighe, E. Woldhuis, J. J. C. Remmers, W. van Saarloos, and M. van Hecke, Phys. Rev. Lett. **105**, 088303 (2010).
[31] K. N. Nordstrom, E. Verneuil, P. E. Arratia, A. Basu, Z. Zhang, A. G. Yodh, J. P. Gollub, and D. J. Durian, Phys. Rev. Lett. **105**, 175701 (2010).
[32] A. Zaccone and E. Scossa-Romano, Phys. Rev. B **83**, 184205 (2011).